Structures 86 (2026) 111392

Contents lists available at ScienceDirect

Structures

journal homepage: www.elsevier.com/locate/structures

High-resolution distributed acoustic sensing for full-scale monitoring of an FRP–concrete composite bridge deck

Evangelia Georgantzia [a,*], Hammed O. Aminulai [b], Duncan Crump [c], David Milne [b], Ali Masoudi [d], Timothy Lee [d], Martynas Beresna [d], Gilberto Brambilla [d], William Powrie [b], Mohammad M. Kashani [b]

[a] School of Civil, Aerospace and Design Engineering, Faculty of Science and Engineering, University of Bristol, Bristol, BS8 1TR, United Kingdom
[b] Boldrewood Innovation Campus, School of Engineering, Faculty of Engineering and Physical Sciences, University of Southampton, Building 178, Southampton SO16 7QF, United Kingdom
[c] Large-Scale Structural Testing Laboratory (LSTL), Boldrewood Innovation Campus, School of Engineering, Faculty of Engineering and Physical Sciences, University of Southampton, Building 178, Southampton SO16 7QF, United Kingdom
[d] Optoelectronics Research Centre (ORC), University of Southampton, University Road, Southampton SO17 1BJ, United Kingdom

ARTICLE INFO

Keywords:
FRP composite bridge
Distributed fibre optic sensors
High resolution
Finite element analysis
Dynamic strain measurement
Structural health monitoring
High-resolution distributed acoustic sensor, HR-DAS
Ultra-low-loss enhanced back-reflecting fibre, ULEB

ABSTRACT

This study presents a combined experimental and numerical validation of a high-resolution distributed acoustic sensing (HR-DAS) system for continuous strain monitoring in a full-scale fibre-reinforced polymer (FRP)–concrete composite bridge deck. The deck specimen, representative of a typical road bridge configuration, comprised a glass-carbon FRP trapezoidal girder integrated with a cast-in-place concrete slab. A four-point quasi-static bending test was conducted to assess the performance of HR-DAS in capturing distributed strain profiles along the girder. Five ultra-low-loss enhanced back-reflecting (ULEB) optical fibres with embedded reflectors were bonded to the girder surface and interrogated using an HR-DAS system. Conventional sensors, including strain gauges and linear variable differential transformers (LVDTs), were used in parallel for validation. A 3D finite element model (FE) was developed in ABAQUS and validated against experimental strain and deflection data. Close correlation was observed between HR-DAS measurements, strain gauges, LVDTs, and FE predictions, with strain and deflection ratios showing mean errors within 10 %. Additionally, the HR-DAS system demonstrated capability for capturing spatiotemporal strain profiles with a 1 kHz sampling rate. These results confirm the accuracy, resolution, and scalability of HR-DAS for structural health monitoring of FRP–concrete composite bridge structures, supporting its application in long-term, real-time monitoring under service conditions.

1. Introduction

1.1. Background and context

Fibre-reinforced polymer (FRP) composite bridges offer several advantages over traditional materials, including a high strength-to-weight ratio, corrosion resistance, and ease of transport and installation [1,2]. However, their long-term structural performance under service conditions remains less well understood due to their relatively recent adoption in civil infrastructure. Unlike conventional materials such as steel or concrete, FRP composites exhibit distinct failure modes, such as delamination, fibre rupture, and matrix cracking, that may occur without obvious external signs [3–7]. Their anisotropic and layered nature also complicates the prediction of behaviour under complex loading conditions. Environmental factors such as ultraviolet radiation exposure, moisture ingress, and temperature fluctuations further impact their durability. Given these uncertainties, continuous structural monitoring is essential to ensure the safety, reliability, and longevity of FRP bridge systems [8–10]. Effective monitoring facilitates early damage detection, validates design assumptions, and supports informed maintenance planning, key factors in promoting the widespread adoption of FRP composite infrastructure.

* Corresponding author.
E-mail addresses: evangelia.georgantzia@bristol.ac.uk (E. Georgantzia), h.o.aminulai@soton.ac.uk (H.O. Aminulai), d.a.crump@soton.ac.uk (D. Crump), d.milne@soton.ac.uk (D. Milne), a.masoudi@soton.ac.uk (A. Masoudi), timothy.lee@soton.ac.uk (T. Lee), m.beresna@soton.ac.uk (M. Beresna), gb2@orc.soton.ac.uk (G. Brambilla), w.powrie@soton.ac.uk (W. Powrie), mehdi.kashani@soton.ac.uk (M.M. Kashani).

https://doi.org/10.1016/j.istruc.2026.111392
Received 15 August 2025; Received in revised form 21 December 2025; Accepted 12 February 2026
Available online 16 February 2026

Numerous sensing techniques have been developed for the structural health monitoring (SHM) of FRP composite structures to capture their complex and often localised failure mechanisms. Traditional methods include strain gauges and linear variable differential transformers (LVDTs), which provide point-based measurements of strain and displacement. More advanced techniques, such as fibre Bragg grating (FBG) array and distributed fibre optic sensors (DFOS), offer greater coverage and the ability to monitor strain and temperature over extended lengths [11–14]. Acoustic emission methods are widely used for detecting damage initiation and progression, particularly delamination and fibre breakage [15–18]. Infrared thermography and ultrasonic testing provide non-contact and non-destructive evaluation of subsurface defects [19,20]. These diverse sensing technologies, often used in combination, enable comprehensive and real-time assessment of FRP structural performance, supporting early damage detection, informed maintenance, and improved safety throughout a structure's lifecycle.

Among these techniques, DFOS has emerged as a powerful tool for monitoring FRP composite structures due to its ability to provide continuous strain measurements along the entire length of an optical fibre. Unlike traditional point sensors, DFOS systems, based on Rayleigh, Brillouin, or Raman scattering, enable detailed strain and temperature profiling over large areas with minimal intrusion [21]. This capability is particularly valuable in FRP composites, where damage such as matrix cracking, delamination, or fibre breakage may occur unpredictably and at localised points. DFOS can be embedded within or retrofitted on FRP components, making it suitable for both laboratory testing and long-term in-situ monitoring. The technology has been successfully applied in various civil engineering applications, including bridge decks [22], pipelines [23], wind turbine blades [24], and railway track [25] enabling early damage detection, real-time assessment, and predictive maintenance. Recent advancements in fibre technology and interrogation systems have further improved the resolution, accuracy, and durability of DFOS, positioning it as a practical and effective solution for comprehensive SHM of FRP structures.

Over the past decade, numerous Fibre Optic Sensing techniques have been implemented for the SHM of FRP composite bridges. One of the earliest examples is the Tech 21 Bridge in the United States, which has undergone long-term monitoring to assess its structural performance over time [26]. In another case, FBG sensors were embedded during the fabrication of the West Mill Bridge in the UK, one of the first FRP composite bridges, as part of its integrated monitoring system. Data collection and performance evaluation for this bridge began approximately three years after construction [27]. Mufti [28] has reported on several FRP composite bridges in Canada that are currently being monitored. In these cases, FBG sensors have primarily been employed to track strain and temperature, providing valuable data on structural performance both during the construction phase and under live traffic conditions. Siwowski et al. [29] present a pilot application of an Optical Frequency-Domain Reflectometry (OFDR) system as the primary SHM method for Poland's first FRP composite bridge. The system's high-resolution, continuous strain and deflection measurements were validated against traditional sensors and finite element (FE) analysis, demonstrating its effectiveness for detecting localised damage and enabling long-term SHM of FRP infrastructure.

More recently, high-resolution distributed acoustic sensing (HR-DAS) has emerged as a powerful tool for full-field strain measurement with high temporal and spatial resolution [30]. The high sampling rate and spatial density of HR-DAS enable precise measurement of dynamic structural responses under various loading scenarios, including controlled laboratory ramp tests and real-world conditions such as live vehicular traffic.

The HR-DAS system was selected in this study due to its overall advantages compared with OFDR and FBG array systems. Table 1 compares the three systems in terms of strain resolution, spatial resolution, number of sensing nodes, maximum sending length and typical dynamic bandwidth. In terms of the practical limitations, it is worth noting that OFDR's sensing range and very low temporal resolution restrict its use to applications involving slow mechanical or thermal changes, such as material characterisation or static load tests. FBG array systems occupy an intermediate position between fully distributed and point-based sensing. By offering discrete strain measurements at selected locations, FBGs are well suited to applications where the monitoring of specific critical points is sufficient, such as modal testing, low-frequency vibration monitoring, and long-term strain measurement in bridges and buildings. Their practical use in dynamic applications is constrained by a trade-off between sampling rate and the number of gratings that can be multiplexed on a single fibre, which limits spatial coverage when high temporal resolution is required. In contrast, HR-DAS enables fully distributed strain or vibration measurements over long distances with high spatial density and high temporal resolution, making it particularly suitable for large-scale infrastructure monitoring. Its ability to capture both quasi-static and dynamic strain responses allows HR-DAS to support applications such as traffic-induced vibration monitoring, impact detection, distributed modal identification, and the detection of localised high-frequency strain transients. These capabilities make HR-DAS especially attractive for bridges where continuous spatial coverage and dynamic response monitoring are required. While HR-DAS involves higher data volumes and more complex interrogation systems, its versatility and scalability offer significant advantages for integrated, multi-functional structural health monitoring.

Table 1
Comparison between HR-DAS, OFDR and FBG array systems.

Component	HR-DAS	OFDR	FBG
Strain resolution	0.001 με	1 με	1 με
Spatial resolution	20 mm	10 mm	Quasi-distributed
Number of sensing nodes	10,000	7000	100
Maximum sensing length	40 km	30 m	10 km
Typical dynamic bandwidth	500 kHz	5 Hz	2 kHz

1.2. Research contribution and novelty

This study investigates, for the first time, the application and validation of an HR-DAS system for SHM of a full-scale FRP–concrete composite bridge deck. The 6000 mm × 2000 mm × 700 mm deck specimen, representative of a typical road bridge section, consisted of a trapezoidal glass-carbon FRP girder integrated with a precast concrete slab. A quasi-static, non-destructive four-point bending test was conducted, focusing solely on validating the HR-DAS system. Conventional discrete/point instrumentation, such as LVDTs and strain gauges, was deployed alongside five 6 m ultra-low-loss enhanced back-reflecting (ULEB) optical fibres with embedded reflectors spaced at 150 mm, interrogated using an HR-DAS system [31]. The aim was to assess, for the first time, the capability of the HR-DAS to measure distributed strain profiles with high spatial resolution on a bridge component. A detailed 3D FE model was developed in ABAQUS [32], incorporating realistic material models and boundary conditions, and was validated against experimental strain and deflection data. This combined experimental–numerical approach was designed to rigorously evaluate the accuracy, resolution, and practicality of HR-DAS for the continuous monitoring of large-scale composite bridge structures.

2. Sensing principle of high-resolution distributed acoustic sensor (HR-DAS)

HR-DAS is an optical fibre sensing technology that enables strain variation along an optical fibre to be spatially and temporally characterised. For instance, an HR-DAS system with a 10 cm gauge length can transform a 1000 m fibre into an array of 10,000 strain gauges, offering high-resolution, distributed strain measurements.

HR-DAS operates on the basis of an optical interrogation method known as Optical Time-Domain Reflectometry (OTDR). In this technique, short optical pulses are launched into one end of the fibre. As these pulses propagate through the fibre, a small fraction of the light is reflected at each reflector as illustrated in Fig. 1**(a)**. These reflectors are inscribed in the core of the fibre using a femtosecond laser [30]. The reflected signals travel back toward the input end of the fibre. Because the reflectors are spatially distributed, the reflected light from each reflector arrives at the detector at slightly different times, forming a time-resolved signal commonly referred to as an *OTDR trace*. Each point on the OTDR trace corresponds to a specific physical section of the fibre. Any variations in the signal at each point on the OTDR trace indicate changes in the external environment at the corresponding point on the fibre.

The sensing principle of HR-DAS is illustrated in Fig. 1**(b)**. The system extracts the phase of the reflected light from the individual reflectors. To quantify strain over a given section of the fibre, the HR-DAS measures the phase difference between the reflections from a pair of reflectors separated by a distance l. The phase difference $\Delta\varphi$ between the two reflected signals is given by [33]:

$$\Delta\phi = \phi_b - \phi_a = \frac{4\pi n}{\lambda}\xi l \tag{1}$$

where λ is the wavelength of the probe light, n is the refractive index of the fibre, and ξ is the correction factor for the optical path length-change that accounts for strain optic effects ($\xi = 0.79$ at c-band wavelengths). If the length of the fibre between the reflector pair changes by Δl metres, the new phase difference becomes:

$$\overline{\Delta\phi} = \overline{\phi_b} - \overline{\phi_a} = \frac{4\pi n}{\lambda}\xi(l + \Delta l) \tag{2}$$

Subtracting Eq. (1) from Eq. (2) yields the change in phase difference as shown in Eq. (3):

$$\overline{\Delta\phi} - \Delta\phi = \frac{4\pi n}{\lambda}\xi\Delta l \tag{3}$$

Eq. (3) shows that the change in phase difference is linearly proportional to the change in distance between the reflectors. By continuously launching probe pulses into the fibre and tracking the evolution of phase differences between reflector pairs, HR-DAS enables precise measurement of dynamic strain with nano-strain accuracy.

3. Experimental programme

The main objective of the experimental program was to determine the ability of the HR-DAS to measure strain profiles along the composite bridge deck. Thus, a full-scale non-destructive four-point bending test was performed at the National Infrastructure Laboratory at the University of Southampton.

3.1. Full-scale test specimen

The prototype full-scale FRP–concrete composite bridge deck, measuring 6000 mm × 2000 mm × 710 mm and weighing approximately 9.5 tons, was designed and manufactured in a manner similar to the previous study [34]. The deck was designed to be representative of a road bridge deck with a single girder section. The deck consists of two main parts: a glass-carbon FRP composite shell with open, trapezoidal cross-section (girder) and a concrete slab. Fig. 2 presents the geometric details of the girder cross-section. The glass-carbon FRP shell was manufactured using vacuum infusion within a 3D-printed polymer female mould. Its structural configuration included solid E-glass top flanges composed of alternating ±45° and 0° E-glass layers, foam-core webs with balanced ±45° E-glass face sheets, and a predominantly unidirectional carbon fibre bottom flange. The ±45° face sheets of the webs were laid continuously along the inner and outer surfaces of the girder cross-section to facilitate effective shear transfer between the webs and the top flanges. As shown in Fig. 2, the web sandwiched a 38 mm thick PET foam core to increase resistance to out-of-plane movement and web buckling. At the base of the web, these ±45° face sheets were spliced using an equal number of alternating ±45° layers interleaved with 0° carbon fabric layers. The resin system employed was Derakane 610c (Ashland Global), an epoxy-vinylester blend known for its high durability and toughness [34]. More details on the materials properties can be found in the official report of the previous study [35].

The concrete slab, 200 mm thick, was cast on the FRP girder and connected using friction-type shear connectors. The geometric and reinforcement details of the deck specimen are illustrated in the plan, elevation, and cross-sectional views (Section A–A) in Fig. 3. The shear connectors consisted of ASTM A193 grade B8 threaded rods with details as shown in Fig. 3**(c)** and spaced at 305 mm. Unlike discrete connectors such as studs or bolts, these friction-type connectors rely on the

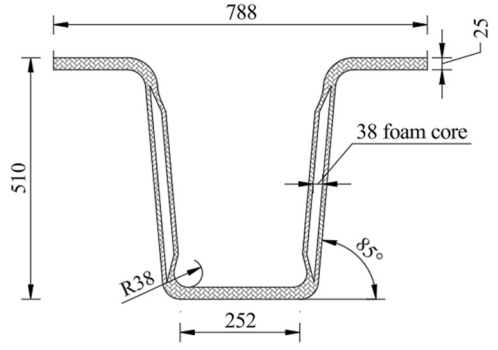

Fig. 2. Geometric properties of the glass-carbon FRP composite girder (units: mm) (adapted from [34]).

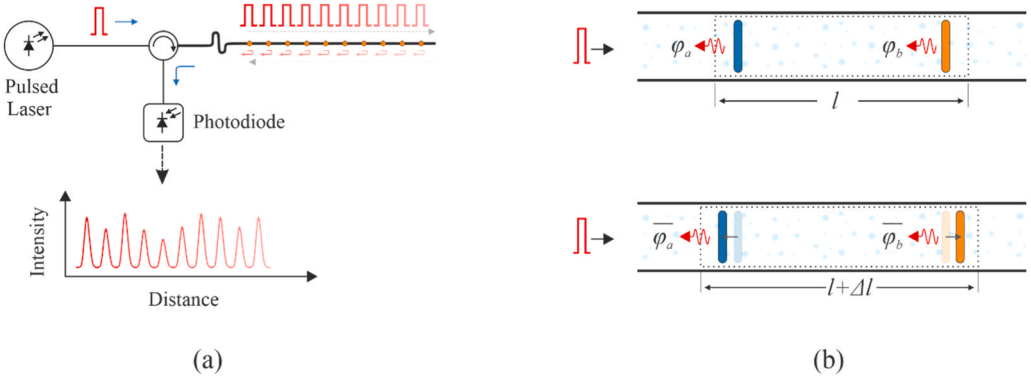

Fig. 1. a) Principle of Optical Time-domain Reflectometry (OTDR); b) Principle of strain measurement in ULEB fibre using High-Resolution DAS (HR-DAS) system.

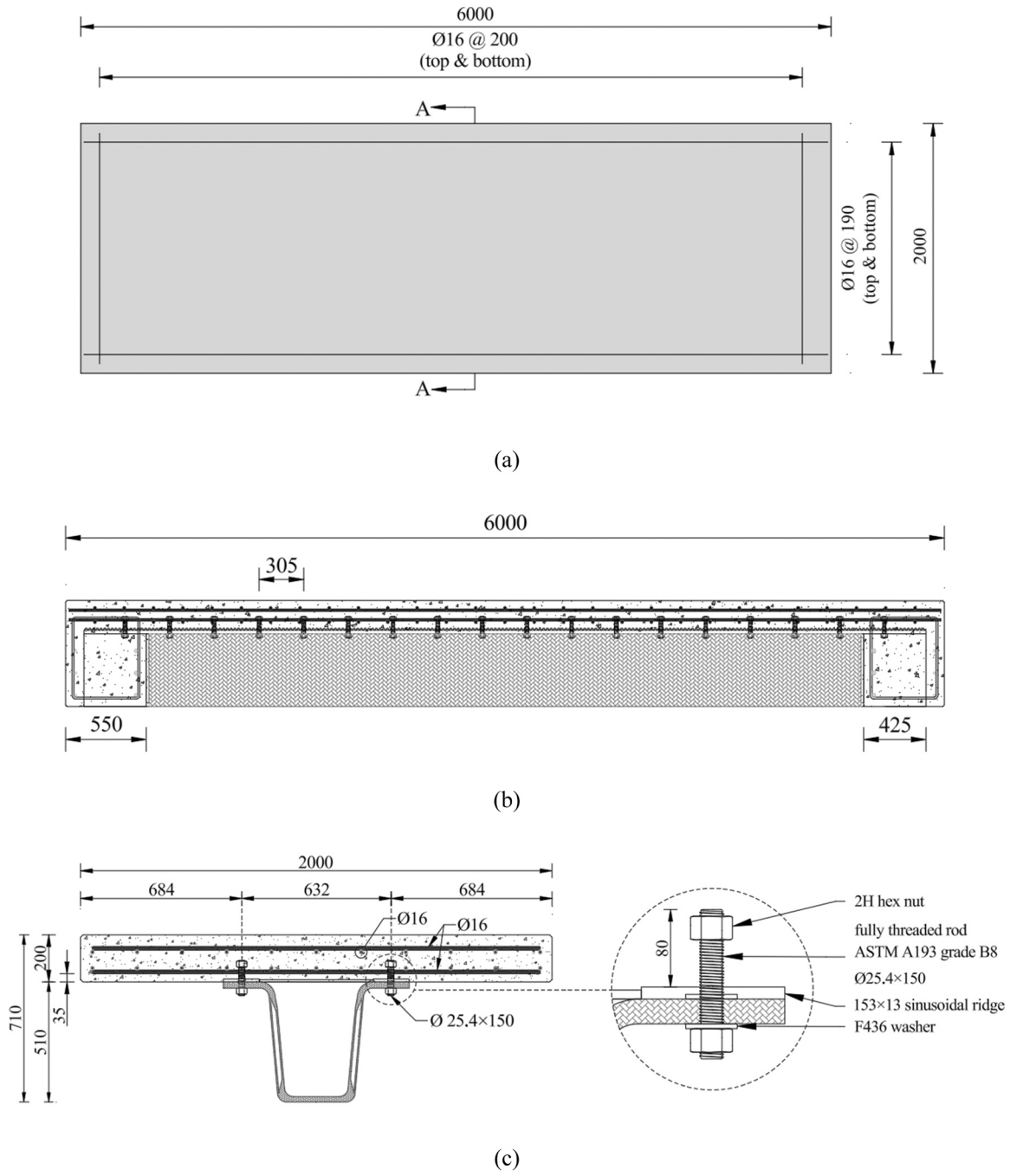

Fig. 3. Geometric and reinforcement details of the FRP–concrete composite bridge deck specimen; (a) elevation view, (b) plan view and (c) section A-A (units: mm).

intentionally roughened or deformed upper surfaces of the girder flanges. Shear transfer is achieved through the mechanical interlock between the cast-in-place concrete deck and the irregular flange surface, which resists longitudinal slip at the FRP–concrete interface and enables composite action between the girder and the slab [36]. The irregular flange surface was created during infusion using a high-density polyethylene caul plate, with sinusoidal ridges 12.7 mm in height machined across its width (Fig. 3**(c)**). Fig. 4 shows a photograph of the glass-carbon FRP composite girder before concrete casting. All thickness values refer to the mid-span of the girder. To accommodate higher shear demands near the supports, the web thickness of the girder was locally increased to 7.3 mm [34]. Additionally, unidirectional carbon fibre layers were selectively omitted at three locations along each half-span, in accordance [34]. A 550 mm-thick backwall, matching the girder height and spanning the full width of the deck, was cast at each end of the girder prior to deck installation and grouting (Fig. 3**(b)**). The backwall was securely connected to the girder using the same ASTM A193 grade B8 threaded rods employed for the girder-to-deck connection.

3.2. *Mechanical properties of materials*

To determine the compressive strength of the concrete used in the deck slab and backwalls, four standard 100 mm × 100 mm × 100 mm cubes were cast from the same mix. The specimens were kept in a rest period for 24 h before being demoulded and placed in a water tank at ambient temperature for curing. On the day of the structural testing, the cubes were tested under axial compression according to [37], resulting

Fig. 4. Photograph of the glass-carbon FRP composite girder before concrete casting.

in an average compressive strength of 78.22 MPa. The concrete slab was reinforced with ASTM A955 Grade 60 stainless steel bars, with a nominal yield strength of 414 MPa [34]. The elastic moduli and ultimate tensile and compressive strengths of the FRP were computed using classical lamination theory, which accounted for fiber orientation and the mechanical properties of both fibers and resin, as reported in the previous study [34]. The shear strength of the FRP web was determined from coupon tests conducted in accordance with ASTM D3518 [38], also described in [34]. The key mechanical properties of the FRP materials for different components of the girder are summarised in Table 2.

3.3. Test set-up

Figs. 5 and 6 illustrate a schematic diagram and a photograph of the four-point test setup, respectively. The tests were performed around the 30 m × 15 m strong floor, which was set up to enable the large test. Unlike a standard test machine, the strong floor acts as part of the 'test loop' to react to the forces imparted to the test specimen. The specimen was simply supported on a pair of 'floor beams' which were rigidly connected to the strong floor via large pre-tensioned Macalloy bolts. The strong floor has attachment points for steelwork on a 1 m × 1 m grid and thus the 'floor beams' were positioned 2.65 m off the centre of the specimen. To avoid any potential localised failure of the concrete backwalls, SKE laminated elastomeric bearings (600 mm × 400 mm × 50 mm) were placed between the specimen and the floor beams (see Fig. 5).

The specimen had a clear span of 4900 mm with a 150 mm overhang on each side, as shown in Fig. 5. Loading was applied using a 500 kN MTS hydraulic actuator via a spreader beam composed of a 305 mm × 305 mm × 137 kg/m I-section, along with two 2.2 m long loading heads made from 203 mm × 204 mm × 86 kg/m I-sections, to impose four-point bending across the full width of the specimen. The actuator was mounted on a portal-type reaction frame specifically designed to operate with the laboratory's strong floor and resist vertical loads exceeding 1 MN (see Fig. 6). The actuator was operated in displacement control mode using MTS AeroPro software, with ram movement controlled at a predefined rate (mm/min). However, the applied force was continuously monitored and used to control or terminate the test upon reaching pre-defined thresholds (further details are provided in Subsection 3.5). The actuator was equipped with an integrated LVDT to measure displacement, and a load cell to record the applied force.

Table 2
Mechanical properties of the FRP materials for different girder components [34].

Component	Longitudinal Modulus [GPa]	Ultimate Compressive Stress [MPa]	Ultimate Shear Stress [MPa]	Ultimate Tensile Stress [MPa]
FRP-Top Flange	27.1	375	–	–
FRP-Web	15.4	–	68.9	205
FRP-Bottom Flange	77.5	–	–	765

3.4. Instrumentation

3.4.1. Conventional

Alongside the built-in LVDT and load cell on the actuator, the test specimen was instrumented with standalone LVDTs and strain gauges to measure deflections and longitudinal strains, respectively. The exact locations of the LVDTs and strain gauges are shown in Figs. 5 and 7. A total of five LVDTs were installed at discrete points along the underside of the glass-carbon FRP girder; one at midspan, one directly beneath each loading point, and one at the midpoint between each loading point and the adjacent support. A total of fourteen 60 mm linear wire strain gauges were bonded to the glass-carbon FRP girder and the concrete slab in the vicinity of the midspan. The gauges were positioned at various heights from the girder flange to facilitate identification of the neutral axis, and were distributed on both sides of the specimen (see Fig. 7). Fig. 8 presents a photograph of the applied instrumentation. All instrumentation, including the actuator's in-built sensors, LVDTs, and strain gauges, was connected to a Vishay Strainsmart 8000 data acquisition system, which recorded data at a frequency of 100 Hz throughout the tests.

3.4.2. HR-DAS

In addition to the traditional sensors, an HR-DAS was also employed to map the strain distribution over the entire length of the girder [30]. The HR-DAS system consists of two main components for strain mapping:

- An ultra-low-loss enhanced back-reflecting (ULEB) optical fibre, incorporating discrete reflectors with 150 mm spacing.
- An interrogator.

To map the strain distribution along the entire girder, five 5 m-long ULEB fibres, each with reflectors spaced at 150 mm intervals, were bonded to the exterior surface of the girder using spray adhesive, following the layout shown in Figs. 5 and 7. The fibres were spliced to one another to allow the interrogation of all reflectors with a single HR-DAS interrogator. The probe pulse repetition rate was set to 1 kHz, and the reflectors were continuously sampled throughout the structural testing. Fig. 8 shows two of the installed ULEB fibres, HR-DAS/4 and HR-DAS/5.

3.5. Proof loading protocol

The specimen was subjected to a maximum load of 495 kN at a cross-head displacement rate of 1.2 mm/min. This load level was chosen to simulate the characteristic LM-1 loading according to EN 1991–2 [39]. The loading procedure consisted of a stepped incremental quasi-static load, hold, and reload pattern, allowing for visual inspection of the specimen. Particularly, the specimen was held at five different load levels, i.e. 100 kN, 200 kN, 300 kN, 400 kN and 495 kN.

4. 3D linear FE modelling

The primary advantage of HR-DAS is its ability to capture continuous strain distribution along the entire length of the bridge deck, whereas conventional strain gauges record longitudinal strains at discrete

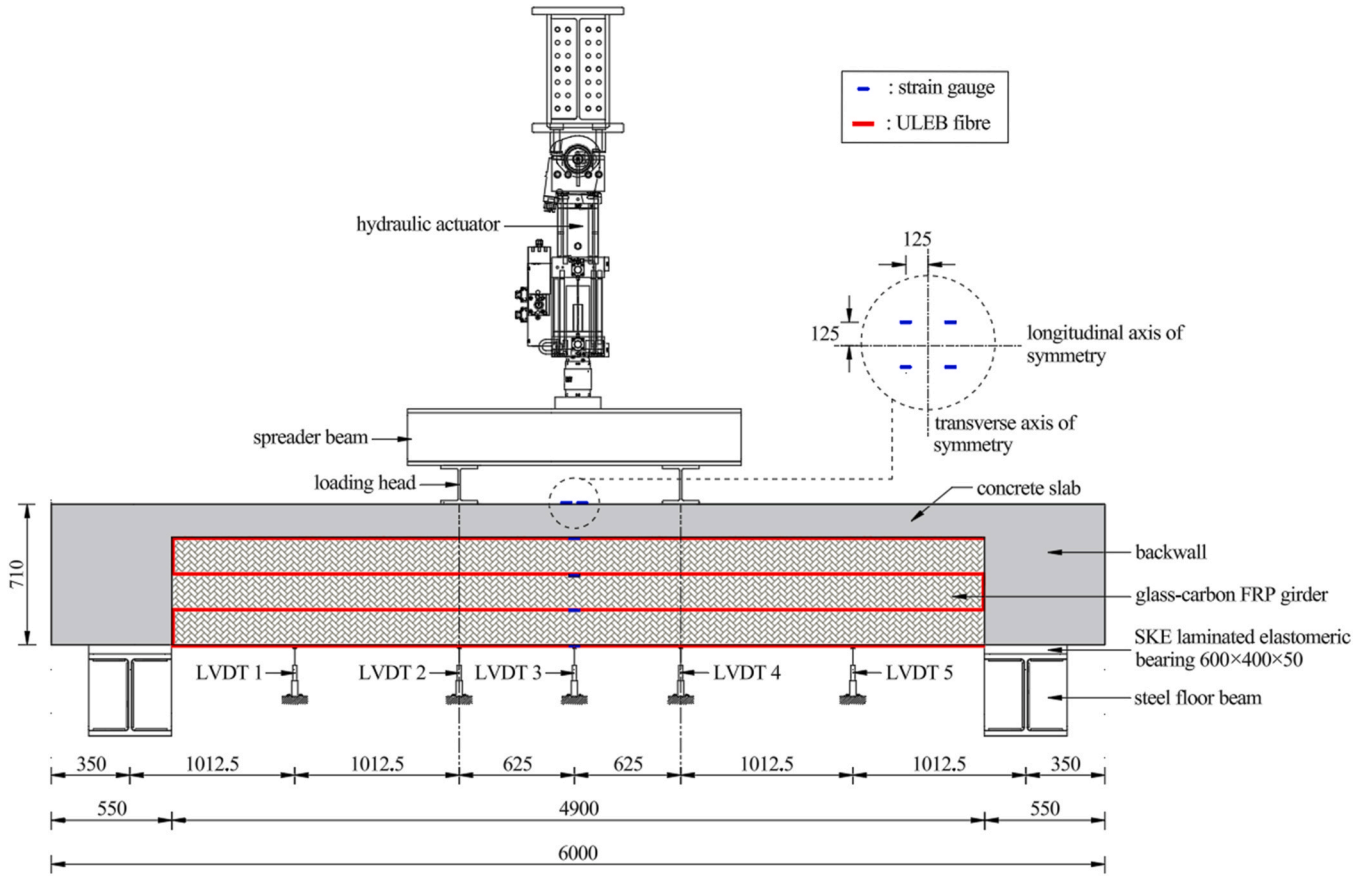

Fig. 5. Schematic illustration of the four-point bending test setup (units: mm).

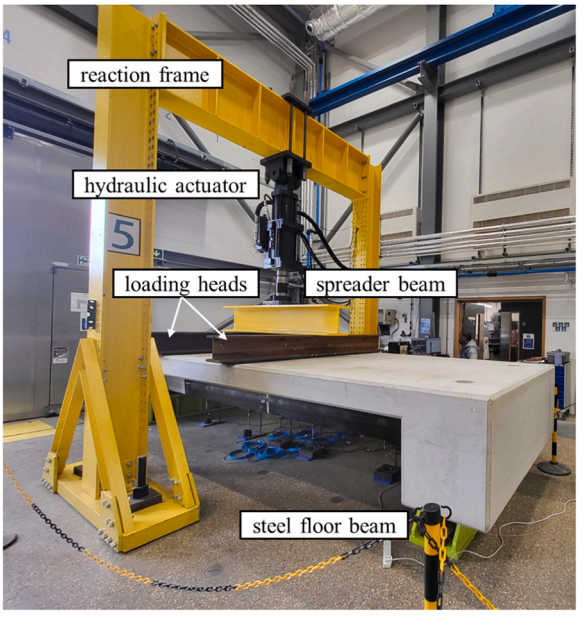

Fig. 6. Photograph of the four-point bending test setup.

locations. Therefore, it is appropriate to develop an FE model of the tested specimen, validate it against the experimental results, and subsequently use it to assess the accuracy of the HR-DAS technology in measuring strain profiles along the deck. It should be noted that material nonlinearity was not considered in this study because the developed strains in the various materials remained in the linear elastic range.

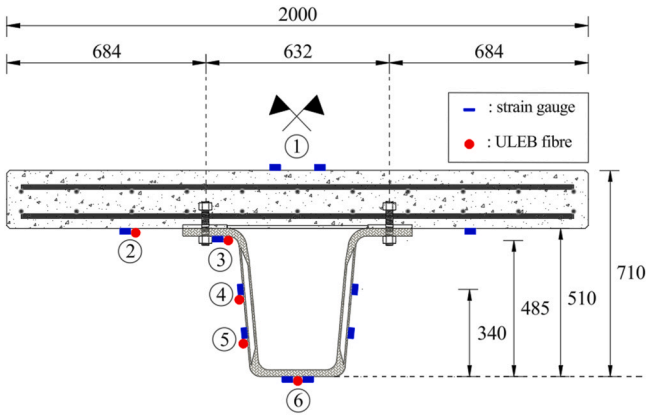

Fig. 7. Details of the instrumentation at the mid-span of the FRP–concrete composite bridge deck specimen (units: mm).

4.1. General assumptions and methodology

The linear FE model of the bridge deck was developed in ABAQUS [32] and is illustrated in Fig. 9. The concrete components (slab and backwalls) were modelled with three-dimensional, linear, reduced integration, 8-node linear brick elements with three degrees of freedom per node (C3D8R) [40]. These were assigned isotropic, linearly elastic constitutive behaviour with Young's modulus calculated based on EN 1992–1–1 [41] and using the average compressive strength obtained from tests (see Subsection 3.2). Poisson's ratio was taken equal to 0.2 [41]. Like the concrete components, the steel components (spreader beam and loading heads) and the glass-carbon FRP girder were modelled

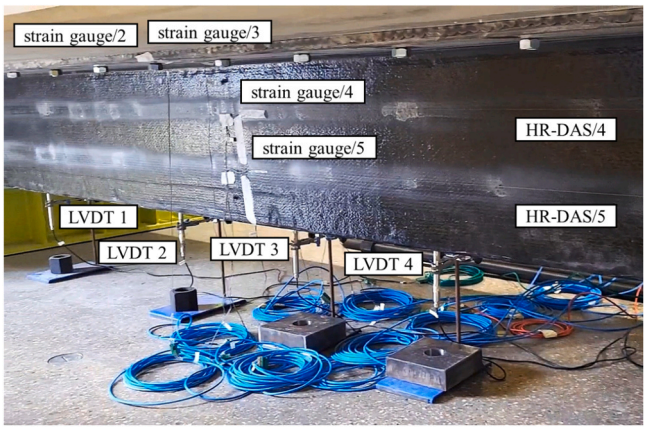

Fig. 8. Photograph of the applied instrumentation at the mid-span of the FRP–concrete composite bridge deck specimen.

with C3D8R elements. The reinforcing steel bars embedded within the deck slab were modelled with 2-node linear displacement truss elements with three degrees of freedom per node (T3D2). All steel components were assigned isotropic, linearly elastic constitutive behaviour with Young's modulus and Poisson's ratio equal to 210 GPa and 0.3, respectively [42]. The same constitutive material model was adopted for the elements making up the girder's top flanges, webs, and bottom flanges, with their specific laminate properties taken from Table 2. Aiming to minimise the computational time without compromising the accuracy of the results, a mesh convergence study was conducted, resulting in a uniform mesh with a size equal to 50 mm × 50 mm. The concrete slab, glass-carbon FRP girder and backwalls were connected using tie constraints, assuming perfect bonding –no slip, no separation– as negligible deformations were expected when using shear-friction connections [36]. Surface-to-surface contact was used to model the interaction between the spreader beam and the loading heads, the loading heads and the concrete slab, and the backwalls and the elastomeric bearings. "Hard contact", which allows for separation of both surfaces in tension and prevents penetration in compression was employed in the normal direction. The Coulomb friction model was used in the tangential direction with a friction coefficient value of 0.30. An "embedded region" constraint was defined to embed the reinforcing bars into the concrete slab. Moreover, reference points (RPs) were created at the geometric centre of the bottom end surfaces of the bearings to apply the boundary conditions. The degrees of freedom (DOFs) between the RPs and the corresponding end surfaces were coupled using rigid body constraints. The DOFs of both RPs were restrained to simulate the support conditions employed in the test (see Fig. 9). The load was applied as "pressure" on the top flange of the spreader beam as shown in Fig. 9. Finally, linear static analysis with small displacements was chosen to capture the bending response of the FRP–concrete composite bridge deck under the considered load.

4.2. Model validation

Adopting the aforementioned modelling assumptions, the developed FE model was validated by comparing its results with the corresponding experimental data. Three of the total six strain gauges (bottom of the concrete slab, lower web and bottom flange of the glass-carbon FRP girder) were excluded from the validation process due to unreliable readings, which were attributed to bonding failures during installation. For the remaining strain gauges, the load–longitudinal strain curves at mid-span from both the experiments and the FE model are presented in Fig. 10. The ratios of numerical to experimental longitudinal strain at the maximum applied load of 495 kN are reported in Table 3. The resulting mean value is 0.97, with a coefficient of variation (COV) of 0.03, indicating accurate and consistent numerical predictions.

Furthermore, deflection measurements were used to validate the developed FE model. Specifically, deflection values recorded by LVDTs 1–3 were compared to corresponding values obtained numerically – measurements from LVDT 4 and LVDT 5 were the same as those from LVDT 2 and LVDT 1, respectively. It is noted that the experimental deflections exclude any deformation within the layered elastomeric bearing pads. Fig. 11 presents the load–deflection response at mid-span of the composite deck. Additionally, Table 4 reports the ratios of numerical to experimental deflection at 495 kN, yielding a mean value of 1.12 and a COV of 0.07. Overall, good agreement is observed between experimental and numerical results, indicating that the developed FE model accurately captures the flexural response of the FRP–concrete composite bridge deck under the applied loading conditions. Moreover, Fig. 12 presents the longitudinal strain distribution on the top surface of the concrete slab, plotted across the slab width at the quarter- and mid-span sections. It can be observed that the strains are non-uniformly distributed, with higher values at the centre of the width. In particular, the differences between the edge and mid-width strains are 4.4 % and 10.8 % at the quarter- and mid-span sections, respectively. This non-uniform strain distribution clearly confirms that the composite deck exhibited a shear-lag effect.

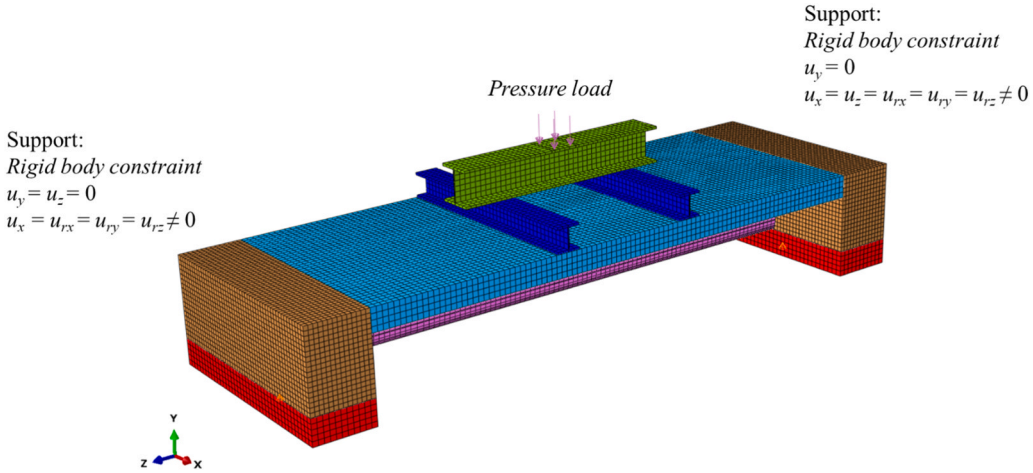

Fig. 9. FE model of the FRP–concrete composite bridge deck.

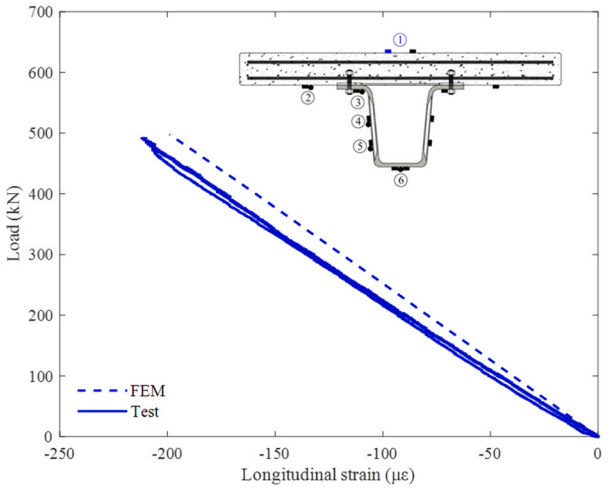

(a)

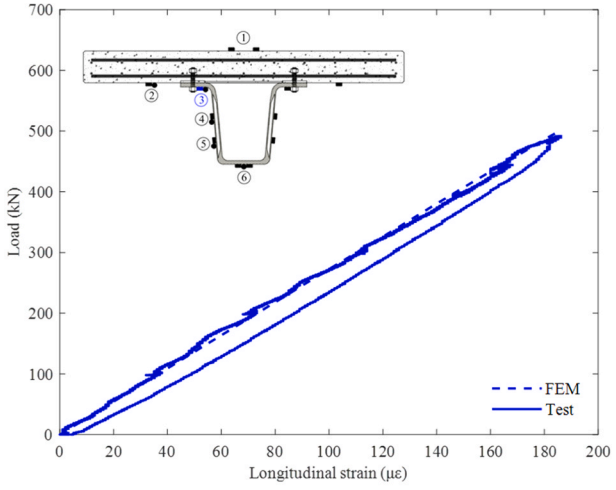

(b)

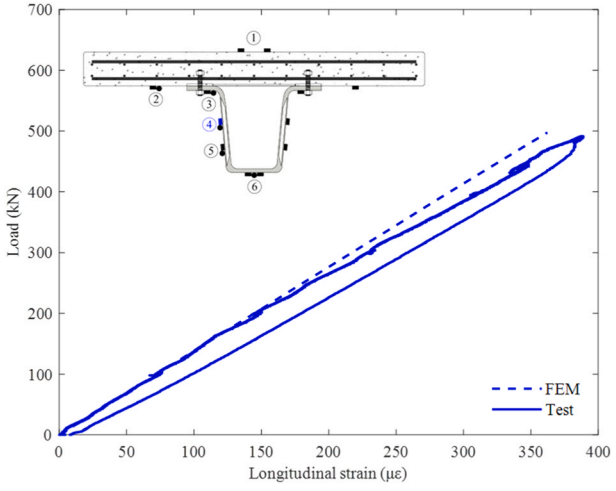

(c)

Fig. 10. Comparison between FE and experimental load–deformation curves at the (a) top of the concrete slab, (b) top flange of the glass-carbon FRP girder and (c) web of the glass-carbon FRP girder.

5. HR-DAS results and discussion

5.1. Validation

5.1.1. Results

Following the validation of the developed FE model against the experimental results collected by the conventional sensors, the model can be used to assess the accuracy of the HR-DAS in measuring strain profiles along the deck. To this end, results obtained by the HR-DAS system and the FE model are compared graphically using spatial-domain plots. This approach offers intuitive engineering insights and highlights qualitative differences between the measurement techniques being compared.

Fig. 13 presents the strain distributions along the length of the glass-carbon FRP girder as recorded by the ULEB fibres OF2 to OF6, shown with continuous lines. The corresponding strain distributions obtained from the FE model are depicted with dashed lines. For comparison, the results from the discrete strain gauges installed at mid-span are also included in the figure and represented by 'square' and 'diamond'. As can be seen from Fig. 13, a good correlation was achieved between the strain results obtained from the HR-DAS technology, strain gauges, and the FE model. Moreover, as shown in Fig. 13, the bottom-flange strain within the constant-moment region varies by 6.2 %. Although this region corresponds to zero global shear force, the deck behaves as a finite-width plate rather than an ideal beam. Free-edge and Poisson-coupling effects induce shear-lag that redistributes longitudinal stresses across the width, while the finite load-patch length introduces local through-thickness bending near the loading points that decays toward mid-span [43,44]. In addition, the discrete connector arrangement causes minor stiffness variations along the span. These three-dimensional plate and local loading effects explain the small longitudinal-strain gradient observed within the constant-moment region and are consistent with previous observations for composite and plate-type structures [45–48]. The FE results remained linear and well-converged, confirming that the observed behaviour represents a genuine structural response rather than a modelling artefact.

To quantitatively assess the accuracy of strain measurements using HR-DAS technology, strains recorded at mid-span are listed in Table 3 and compared with those obtained from the FE model. The ratios of HR-DAS to numerical strains yield a mean value of 1.07 and a COV of 0.09, indicating a slight overestimation of strain by the HR-DAS system, but overall good agreement with the numerical predictions. Additionally, Table 3 includes the ratios of HR-DAS to conventional experimental strain measurements at two mid-span locations, with a mean of 0.96 and a COV of 0.08. These results confirm the high accuracy and consistency of the HR-DAS technology in capturing strain responses, demonstrating its suitability for structural monitoring applications where reliable, high-resolution strain data are required.

To further support this analysis, the absolute longitudinal strain differences between HR-DAS and the FE model, and between HR-DAS and strain gauges, were normalised by the maximum recorded strain and are also included in Table 3. As shown, the differences between the HR-DAS and numerical strains remain consistently below 10 % across the girder web and bottom flange, with a larger difference of 19 % observed at the bottom of the concrete slab. The differences between HR-DAS and strain-gauge measurements at the two mid-span locations were calculated as 4 % and 12 %, respectively. These levels of discrepancy are consistent with typical uncertainties in both experimental measurements and numerical modelling and can be explained in the following subsection.

5.1.2. Error sources

In the HR-DAS technology, the strain transfer between the structure and the optical fibre depends on the quality and thickness of the adhesive and any protective layers. Small imperfections, micro-slip, or partial debonding can attenuate or slightly distort the strain transmitted to the

Table 3
Comparison of longitudinal strains obtained experimentally (strain gauges and HR-DAS) with FEM results.

Measurement location at the mid-span	ε_{SG} [$\times 10^{-6}$]	ε_{FEM} [$\times 10^{-6}$]	ε_{FEM} / ε_{SG}	$\varepsilon_{HR\text{-}DAS}$ [$\times 10^{-6}$]	$\varepsilon_{HR\text{-}DAS}$ / ε_{FEM}	$\lvert\varepsilon_{HR\text{-}DAS} - \varepsilon_{FEM}\rvert$ / max($\varepsilon_{HR\text{-}DAS}$,$\varepsilon_{FEM}$) [%]	$\varepsilon_{HR\text{-}DAS}$ / ε_{SG}	$\lvert\varepsilon_{HR\text{-}DAS} - \varepsilon_{SG}\rvert$ / max($\varepsilon_{HR\text{-}DAS}$,$\varepsilon_{SG}$) [%]
1	-211	-201	0.95	–	–	–	–	–
2	–	129	–	160	1.24	19 %	–	–
3	184	186	1.01	191	1.03	3 %	1.04	4 %
4	386	365	0.95	341	0.93	7 %	0.88	12 %
5	–	541	–	591	1.09	9 %	–	–
6	–	741	–	794	1.07	7 %	–	–
Mean			0.97		1.07		0.96	
COV			0.03		0.09		0.08	

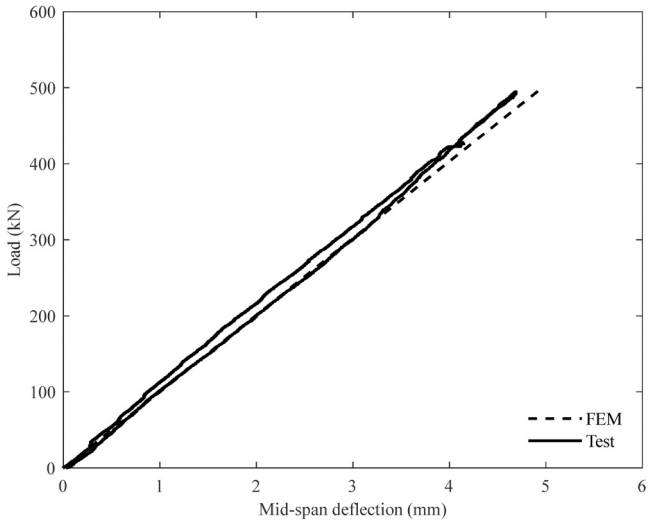

Fig. 11. Comparison between FE and experimental load–deflection curves at the mid-span of the glass-carbon FRP girder.

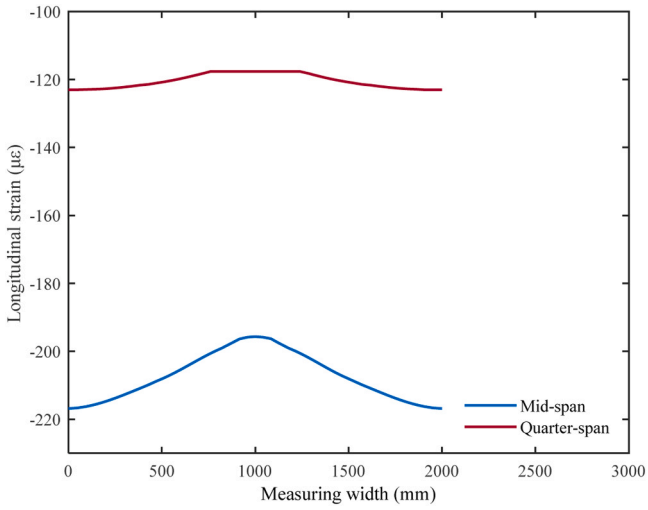

Fig. 12. Longitudinal strain distribution on the top surface of the concrete slab at the quarter- and mid-span sections.

Table 4
Comparison of deflections obtained experimentally with FEM results.

	δ_{LVDT} [mm]	δ_{FEM} [mm]	δ_{FEM} / δ_{LVDT}
LVDT 1	2.27	2.78	1.22
LVDT 2	4.17	4.56	1.09
LVDT 3	4.69	4.93	1.05
Mean			1.12
COV			0.07

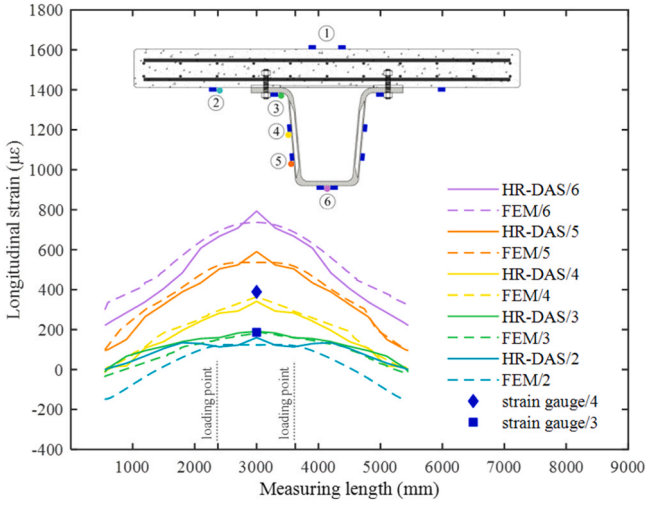

Fig. 13. Comparison between longitudinal strain profiles obtained by the HR-DAS system and FEM.

fibre. Minor surface heterogeneities, particularly in the concrete slab region, may also influence the strain-transfer efficiency, which is consistent with the larger (19 %) difference observed there, even under elastic behaviour.

Moreover, the FE model introduces its own modelling and material idealisations. Global material properties (e.g. elastic modulus of steel, concrete, and glass-carbon FRP materials) were taken from batch-average test data, whereas the actual in-situ stiffness may differ slightly. Assumptions regarding boundary conditions, composite action, and shear connection (e.g. no slip at interfaces, idealised simply-supported conditions) may not perfectly represent the real behaviour. Even within the elastic range, these idealisations can influence the predicted strain distribution, helping to explain the observed discrepancies, particularly in the concrete slab region. Mesh discretisation may provide an additional source of numerical error.

Finally, the differences between HR-DAS and conventional strain gauges (4 % and 12 %) are within the range expected from gauge installation and measurement uncertainties. Bond quality, surface preparation, and adhesive curing influence the effective strain transfer to the gauge. The very small difference (4 %) at one location indicates excellent local agreement, while the higher value (12 %) at the other point remains reasonable given the combined effects of HR-DAS strain-transfer characteristics and conventional gauge installation tolerances.

Overall, the observed discrepancies indicate that HR-DAS can reproduce both numerical and conventional experimental strains within the combined experimental and modelling uncertainty. For design and SHM practice, this suggests that HR-DAS can be expected to capture global bending strains with an accuracy of better than about 10 % under

similar conditions, with larger deviations primarily confined to regions where local material heterogeneity or interface effects influence strain transfer.

5.2. HR-DAS capability for dynamic strain measurement

As noted earlier, a key advantage of using HR-DAS for strain measurement over techniques such as OFDR is its capability to capture dynamic strain variations. The system offers an operational bandwidth exceeding 500 kHz, enabling the recording of high-frequency strain responses associated with dynamic loading, vibrations, or impact events [31]. While such a bandwidth far exceeds that required to capture global bridge dynamics, whose fundamental frequencies typically lie below approximately 10–20 Hz, it is highly relevant for monitoring localised, higher-frequency phenomena. These include traffic-induced impacts, bearing responses, and damage-related mechanisms that may generate strain components extending into the kHz range.

The high temporal resolution of HR-DAS therefore provides the potential to detect high-frequency strain transients, such as those associated with impacts, acoustic emission activity, or early-stage fatigue crack initiation and propagation. Although the present study focuses exclusively on quasi-static behaviour and does not experimentally demonstrate these dynamic capabilities, the results highlight the suitability of HR-DAS for future SHM applications that require simultaneous monitoring of global structural response and local high-frequency events.

In this study, the sampling rate was set to 1 kHz, which was sufficient given the low loading rate of the test. Fig. 14 presents the strain profile measured at the bottom of the glass-carbon FRP girder during the test using sensing nodes on the HR-DAS/6 sensor. Fig. 14**(a)** shows the spatiotemporal response of the girder, where each line in the waterfall plot represents the response of an individual sensing node on HR-DAS/6 over time. Fig. 14**(b)** presents a 2D cross-section of this plot, showing the time-dependent strain signals at three specific locations along the girder: 3000 mm, 1800 mm, and 900 mm measured from the edge of the composite bridge. These results demonstrate that the HR-DAS system can accurately map the strain distribution over time. It should be noted that no dedicated modal or impact testing was performed in this study, and the dynamic content observed here reflects only the quasi-static loading ramp. Nevertheless, the inherent capability of the HR-DAS system to capture highly dynamic strain responses represents a significant advantage for future dynamic and vibration-based SHM applications.

5.3. Potential application of HR-DAS in bridge structural health monitoring

The experimental and numerical results presented in this study demonstrate that HR-DAS can accurately capture distributed strain profiles and spatiotemporal structural response of an FRP–concrete composite bridge deck under elastic service-level loading. Importantly, no material damage was induced, and the core contribution of this work is therefore the validation of HR-DAS as a full-field strain-measurement and model-verification tool, rather than as a damage-detection system. Building on this validated capability, two specific SHM use-cases are identified below where HR-DAS is particularly well suited for FRP–concrete composite bridges, together with the additional work required for each application.

5.3.1. Potential use-case 1: service-level performance monitoring and model validation of FRP–concrete composite decks

HR-DAS is ideally suited for long-term monitoring of FRP–concrete composite bridges operating predominantly within the elastic range. The dense spatial resolution demonstrated in this study enables continuous tracking of longitudinal strain distributions along FRP–concrete composite girders, allowing verification of composite action, identification of shear-lag effects, and detection of changes in global stiffness over time. In this context, HR-DAS can support calibration and updating of FE models used for asset management, load rating, and remaining-life assessment.

Additional work required includes long-term deployment on an in-service bridge under operational traffic and environmental loading to assess durability of fibre bonding, temperature compensation strategies, and data stability over multi-year timescales.

5.3.2. Potential use-case 2: detection of damage initiation and progression under cyclic or extreme loading

Beyond elastic monitoring, HR-DAS has strong potential for detecting damage mechanisms relevant to FRP–concrete systems, such as FRP cracking or delamination, degradation of shear-friction connectors, or loss of composite action at the FRP–concrete interface. The high spatial density and dynamic capability of HR-DAS make it particularly attractive for identifying localised strain anomalies and their temporal evolution during cyclic loading, fatigue, or extreme events (e.g. seismic excitation).

Additional work required includes dedicated laboratory tests involving cyclic or fatigue loading with controlled damage induction, as well as dynamic tests to establish damage-sensitive strain features and thresholds. These studies are necessary to distinguish reversible elastic strain changes from irreversible damage-related signatures and to

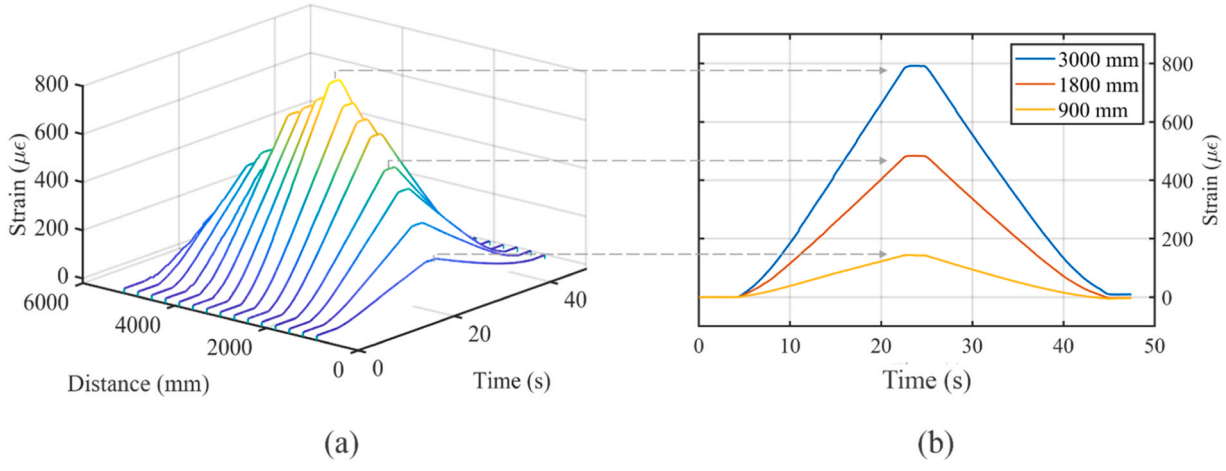

Fig. 14. a) Spatio-temporal profile of the glass-carbon FRP girder; b) 2D cross-section of the spatio-temporal profile for three sensing nodes on the HR-DAS/6 sensor.

quantify detection sensitivity.

Overall, the present study establishes HR-DAS as a robust and scalable sensing technology for elastic-range monitoring and structural model validation of FRP–concrete composite bridges. The targeted use-cases outlined above define a clear pathway for future research aimed at extending HR-DAS toward damage-sensitive and decision-support SHM applications.

6. Conclusions

This study has demonstrated the feasibility and accuracy of an HR-DAS system for structural SHM of a full-scale FRP–concrete composite bridge deck. The main conclusions are as follows:

1. Continuous strain measurement: The HR-DAS system, using ULEB fibres, successfully captured continuous strain profiles along the length of the FRP girder with high spatial resolution. This capability provides a significant advantage over conventional point-based sensors such as strain gauges.
2. Validation through experiments and 3D finite element (FE) modelling: A four-point bending test was conducted and supported by a validated model developed in ABAQUS [32]. HR-DAS measurements showed good correlation with both strain gauge data and FE predictions, with strain and deflection ratios indicating mean discrepancies of less than 10 %.
3. Dynamic response tracking: The HR-DAS system demonstrated the capability to capture spatiotemporal strain distribution during quasi-static loading. While the HR-DAS system features a broad measurement bandwidth exceeding 500 kHz, enabling potential high-fidelity monitoring of fast dynamic events and vibrations, its performance under such high-rate conditions has not yet been experimentally validated in this study.
4. Scalability and practical potential: The system's distributed nature, high resolution, and adaptability to long sensing lengths make it highly suitable for long-term SHM of FRP and hybrid bridge structures, especially for early damage detection and performance validation under service loads.

Overall, this study supports the broader application of HR-DAS in infrastructure monitoring, offering a scalable and reliable sensing solution for next-generation smart bridges.

CRediT authorship contribution statement

Martynas Beresna: Resources, Project administration. **Timothy Lee:** Resources, Project administration. **Ali Masoudi:** Methodology, Investigation, Formal analysis, Data curation. **David Milne:** Methodology, Investigation. **William Powrie:** Writing – review & editing, Supervision, Resources, Funding acquisition. **Gilberto Brambilla:** Resources, Project administration. **Mohammad M. Kashani:** Writing – review & editing, Supervision, Resources, Methodology, Funding acquisition, Conceptualization. **Duncan Crump:** Methodology, Investigation. **Hammed O. Aminulai:** Methodology, Investigation. **Evangelia Georgantzia:** Writing – original draft, Validation, Software, Methodology, Investigation, Formal analysis, Data curation.

Declaration of Competing Interest

The authors declare that they have no known competing financial interests or personal relationships that could have appeared to influence the work reported in this paper.

Acknowledgements

The authors thank National Highways for their professional and financial support for this research through "PHASE 2: National Highways accelerator Development Of Low Carbon, Non Metallic Bridge Structures Using Innovative FRP Materials & Smart Monitoring" funding scheme. The experiments were performed in the LSTL within the National Infrastructure Laboratory, part of the UK Collaboratorium for Research on Infrastructure and Cities, based at the University of Southampton. The help of Mr Andrew Morgan, LSTL Technician, in preparing the test setup is gratefully acknowledged.

References

[1] Zoghi M. The International Handbook of FRP Composites in Civil Engineering. Boca Raton, London, New York: CRC Press, Taylor & Francis Group; 2013.
[2] Uddin N, editor. Developments in Fiber-Reinforced Polymer (FRP) Composites for Civil Engineering. Woodhead Publishing Limited; 2013.
[3] Daniel IM, Gdoutos EE, Abot JL, Wang K-A. Deformation and Failure of Composite Sandwich Structures. J Thermoplast Compos Mater 2003;16:345–64. https://doi.org/10.1177/0892705703016004005.
[4] Wisnom MR. The role of delamination in failure of fibre-reinforced composites. Philos Trans R Soc A Math Phys Eng Sci 2012;370:1850–70. https://doi.org/10.1098/rsta.2011.0441.
[5] Moorthy V, Marappan K. Identification of delamination severity in a tapered FRP composite plate. Compos Struct 2022;299:116054. https://doi.org/10.1016/j.compstruct.2022.116054.
[6] Garg AC. Delamination—a damage mode in composite structures. Eng Fract Mech 1988;29:557–84. https://doi.org/10.1016/0013-7944(88)90181-6.
[7] Evans JT. Analysis and performance of fiber composites (second edition). Materials Science Engineering A 1992;151:115. https://doi.org/10.1016/0921-5093(92)90189-8.
[8] Farhey DN. Instrumentation System Performance for Long-term Bridge Health Monitoring. Struct Health Monit 2006;5:143–53. https://doi.org/10.1177/1475921706057986.
[9] Hollaway LC. A review of the present and future utilisation of FRP composites in the civil infrastructure with reference to their important in-service properties. Constr Build Mater 2010;24:2419–45. https://doi.org/10.1016/j.conbuildmat.2010.04.062.
[10] Sebastian WM, Johnson M. Interpretation of sensor data from in situ tests on a transversely bonded fibre-reinforced polymer road bridge. Struct Health Monit 2019;18:1074–91. https://doi.org/10.1177/1475921718779403.
[11] Rao Y-J. In-fibre Bragg grating sensors. Meas Sci Technol 1997;8:355–75. https://doi.org/10.1088/0957-0233/8/4/002.
[12] Li H-N, Li D-S, Song G-B. Recent applications of fiber optic sensors to health monitoring in civil engineering. Eng Struct 2004;26:1647–57. https://doi.org/10.1016/j.engstruct.2004.05.018.
[13] Enckell M, Glisic B, Myrvoll F, Bergstrand B. Evaluation of a large-scale bridge strain, temperature and crack monitoring with distributed fibre optic sensors. J Civ Struct Health Monit 2011;1:37–46. https://doi.org/10.1007/s13349-011-0004-x.
[14] Casas JR, Cruz PJS. Fiber Optic Sensors for Bridge Monitoring. J Bridge Eng 2003;8:362–73. https://doi.org/10.1061/(ASCE)1084-0702(2003)8:6(362).
[15] Philippidis TP, Assimakopoulou TT. Strength degradation due to fatigue-induced matrix cracking in FRP composites: An acoustic emission predictive model. Compos Sci Technol 2008;68:3272–7. https://doi.org/10.1016/j.compscitech.2008.08.020.
[16] de Oliveira R, Marques AT. Health monitoring of FRP using acoustic emission and artificial neural networks. Comput Struct 2008;86:367–73. https://doi.org/10.1016/j.compstruc.2007.02.015.
[17] Bar HN, Bhat MR, Murthy CRL. Identification of failure modes in GFRP using PVDF sensors: ANN approach. Compos Struct 2004;65:231–7. https://doi.org/10.1016/j.compstruct.2003.10.019.
[18] Godin N, Huguet S, Gaertner R, Salmon L. Clustering of acoustic emission signals collected during tensile tests on unidirectional glass/polyester composite using supervised and unsupervised classifiers. NDT E Int 2004;37:253–64. https://doi.org/10.1016/j.ndteint.2003.09.010.
[19] Quattrocchi A, Freni F, Montanini R. Comparison between air-coupled ultrasonic testing and active thermography for defect identification in composite materials. Nondestruct Test Eval 2021;36:97–112. https://doi.org/10.1080/10589759.2019.1699084.
[20] Sarr CAT, Chataigner S, Gaillet L, Godin N. Nondestructive evaluation of FRP-reinforced structures bonded joints using acousto-ultrasonic: Towards diagnostic of damage state. Constr Build Mater 2021;313:125499. https://doi.org/10.1016/j.conbuildmat.2021.125499.
[21] Hartog AH. An Introduction to Distributed Optical Fibre Sensors. CRC Press; 2017. https://doi.org/10.1201/9781315119014.
[22] Siwowski T, Kaleta D, Rajchel M. Structural behaviour of an all-composite road bridge. Compos Struct 2018;192:555–67. https://doi.org/10.1016/j.compstruct.2018.03.042.
[23] Yasue N., Naruse H., Masuda J.I., Kino H., Nakamura T., Yamaura T. Concrete pipe strain measurement using optical fiber sensor. IEICE Transactions on Electron 200AD;E83-C:468–74.
[24] Glavind L, Olesen IS, Skipper BF, Kristensen M. Fiber-optical grating sensors for wind turbine blades: a review. Opt Eng 2013;52:030901. https://doi.org/10.1117/1.OE.52.3.030901.

[25] Milne D, Masoudi A, Harkness J, Lee B, Watson G, Le Pen L, et al. Mechanically coupled distributed dynamic strain measurement for track systems and earthworks. Transp Geotech 2025;53:101605. https://doi.org/10.1016/j.trgeo.2025.101605.
[26] Foster DC, Richards D, Bogner BR. Design and Installation of Fiber-Reinforced Polymer Composite Bridge. J Compos Constr 2000;4:33–7. https://doi.org/10.1061/(ASCE)1090-0268(2000)4:1(33).
[27] Kister G, Badcock RA, Gebremichael YM, Boyle WJO, Grattan KTV, Fernando GF, et al. Monitoring of an all-composite bridge using Bragg grating sensors. Constr Build Mater 2007;21:1599–604. https://doi.org/10.1016/j.conbuildmat.2006.07.007.
[28] Mufti AA. Structural Health Monitoring of Innovative Canadian Civil Engineering Structures. Struct Health Monit 2002;1:89–103. https://doi.org/10.1177/147592170200100106.
[29] Siwowski T, Rajchel M, Howiacki T, Sieńko R, Bednarski Ł. Distributed fibre optic sensors in FRP composite bridge monitoring: Validation through proof load tests. Eng Struct 2021;246. https://doi.org/10.1016/j.engstruct.2021.113057.
[30] Masoudi A, Lee T, Beresna M, Brambilla G. 10-cm spatial resolution distributed acoustic sensor based on an ultra low-loss enhanced backscattering fiber. Opt Contin 2022;1:2002. https://doi.org/10.1364/OPTCON.468673.
[31] Lee T, Beresna M, Masoudi A, Brambilla G. Enhanced-Backscattering and Enhanced-Backreflection Fibers for Distributed Optical Fiber Sensors. J Light Technol 2023;41:4051–64. https://doi.org/10.1109/JLT.2023.3281136.
[32] ABAQUS standard user's manual. Providence, RI: Dassault Systèmes Simulia Corp.
[33] van Putten LD, Masoudi A, Snook J, Brambilla G. Numerical Modelling of a Distributed Acoustic Sensor Based on Ultra-Low Loss-Enhanced Backscattering Fibers. Sensors 2021;21:6869. https://doi.org/10.3390/s21206869.
[34] Davids WG, Diba A, Dagher HJ, Guzzi D, Schanck AP. Development, assessment and implementation of a novel FRP composite girder bridge. Constr Build Mater 2022;340. https://doi.org/10.1016/j.conbuildmat.2022.127818.
[35] Schanck A., Davids W. Testing, Monitoring, and Analysis of FRP Girder Bridge with Concrete Deck. 2021.
[36] Davids WG, Guzzi D, Schanck AP. Development and Experimental Assessment of Friction-Type Shear Connectors for FRP Bridge Girders with Composite Concrete Decks. Materials 2022;15:3014. https://doi.org/10.3390/ma15093014.
[37] CEN. Testing hardened concrete – Part 3: Compressive strength of test specimens. BS EN 12390-3:2019 (European Committee for Standardization). Brussels, Belgium: CEN; 2019.
[38] ASTM D3518/D3518M-18. Standard Test Method for In-Plane Shear Response of Polymer Matrix Composite Materials by Tensile Test of a ±45° Laminate. West Conshohocken, PA, USA: ASTM International; 2018.
[39] CEN. EN 1991: Eurocode - Actions on structures. Part 2, Traffic load on bridges (European Committee for Standardization). Brussels, Belgium: CEN; 2003.
[40] Alnahhal W, Aref A, Alampalli S. Composite behavior of hybrid FRP-concrete bridge decks on steel girders. Compos Struct 2008;84:29–43. https://doi.org/10.1016/j.compstruct.2007.06.005.
[41] CEN (European Committee for Standardization). EN 1992-1-1: Eurocode 2: Design of concrete structures - Part 1-1: General rules and rules for buildings. 2004.
[42] Chung W, Sotelino ED. Three-dimensional finite element modeling of composite girder bridges. Eng Struct 2006;28:63–71. https://doi.org/10.1016/j.engstruct.2005.05.019.
[43] Paradiso M, Podio-Guidugli P. Consistent derivation of a beam model from the Saint-Venant three-dimensional solution of a beam-like solid. Int J Solids Struct 2019;159:90–110.
[44] Obst M, Wasilewicz P, Adamiec J. Experimental investigation of four-point bending of thin walled open section steel beam loaded and set in the shear center. Sci Rep 2022;12(1):7275.
[45] Zou B, Chen A, Davalos JF, Salim HA. Evaluation of effective flange width by shear lag model for orthotropic FRP bridge decks. Compos Struct 2011;93(2):474–82.
[46] (a) Vallenilla CR. Effective width criteria for composite beams. Eng J (AISC) 1985; 22(1):3–12.(b) Masoudnia R. State of the art of the effective flange width for composite T-beams. Constr Build Mater 2020;244:118303.
[47] Kytölä U, Tulonen J, Laaksonen A. Longitudinal shear in the tension flanges of composite concrete beams made continuous. Struct Concr 2022;23(2):1100–17.
[48] Hasan A, Subh M, Wardeh G. The concrete effective width of a composite I-girder with numerous contact points as shear connectors. Appl Mech 2024;5(1):163–79.